Two-Dimensional Anisotropic Scattering Radiation in a Thermally Developing Poiseuille Flow

Tae-Kuk Kim* and HaeOk Skarda Lee†
University of Minnesota, Minneapolis, Minnesota 55455

Combined heat transfer by laminar convection and two-dimensional radiation in a thermally developing Poiseuille flow between two infinite plane parallel plates is studied. The gray fluid participates radiatively by absorbing, emitting, and anisotropically scattering radiative energy. Effects of the conduction-radiation parameter, scattering albedo, optical height of the channel, diffuse wall reflectivity, and scattering phase function are studied. Results obtained from one-dimensional treatment of the radiative transfer are shown to be quite different from those obtained from two-dimensional radiation analysis, which show significant preheating of the entering fluid. The two-dimensional effects are more pronounced as the channel optical height increases and as the conduction-radiation parameter and the scattering albedo decrease. The scattering phase functions also significantly influence the preheating as the channel optical height increases.

Nomenclature

C_ℓ = expansion coefficients for scattering phase function
C_p = fluid heat capacity
D_h = hydraulic diameter, $2H$
f = phase function asymmetry factor, $C_\ell/3$
G^* = dimensionless average incident radiation
h = heat-transfer coefficient
H = channel height
I^* = dimensionless intensity, $\pi I/(\sigma T_w^4)$
k_f = thermal conductivity of the fluid
K = order of the phase function expansion
L = channel length
L_e = extended x dimension of the calculation domain
MX,MY = number of grid points in x and y directions
N_{cr} = conduction-radiation parameter, $k_f\beta/(4\sigma T_w^3)$
Nu = Nusselt number, hD_h/k_f
Pe = Peclet number, $\rho_f U D_h C_p/k_f$
$P_\ell(\cos\psi)$ = Legendre polynominal of order ℓ
Q_{rw}^* = dimensionless net wall radiative flux
T_0 = temperature of the cold wall or cold fluid
T_w = temperature of the hot wall
T_b^* = dimensionless bulk fluid temperature
T^* = dimensionless temperature, T/T_w
u^* = dimensionless velocity, u/U
U = mean velocity
β = extinction coefficient
ϵ_w = diffuse wall emissivity
ρ = diffuse wall reflectivity, $1-\epsilon_w$
ρ_f = fluid density
μ,ξ = direction cosines in x and y directions
σ = Stefan-Boltzmann constant
τ_e = optical depth of extended x dimension, βL_e
τ_x,τ_y = optical coordinates, βx and βy
τ_{xL},τ_{yH} = optical thicknesses of the channel, βL and βH
$\Phi(\Omega';\Omega)$ = scattering phase function
ψ = scattering angle measured between Ω' and Ω
θ = dimensionless similarity temperature, $(T_w-T)/(T_w-T_b)$
ω = scattering albedo
Ω = angular direction
ζ = dimensionless x coordinate, $2\tau_{yH}\tau_x/Pe$

Presented as Paper 89-1719 at the AIAA 24th Thermophysics Conference, Buffalo, New York, June 12-14, 1989; received June 14, 1989; revision received Oct. 2, 1989.

*Graduate Student, Department of Mechanical Engineering.
†Assistant Professor, Department of Mechanical Engineering. Member AIAA.

Introduction

THE heat transfer in many high-temperature applications is achieved by a combination of radiative, convective, and conductive heat-transfer modes. Analyses of such applications are often complicated by irregular geometry, turbulence, and combustion. This work is an attempt to study the fundamental interactions of radiation and forced convection by considering a very simple flowfield: a hydrodynamically fully developed laminar flow in an infinite plane parallel channel. Detailed treatment of the radiation heat transfer is achieved by using the accurate S-N discrete ordinates method. Full effects of the anisotropic scattering particles in a fluid can be investigated for a two-dimensional rectangular geometry with this method.[1,2]

A schematic of the system geometry is shown in Fig. 1a. The cold fluid entering the channel is gray and is at an absolute temperature of T_0, where T_0 is set equal to zero for this study. The fluid absorbs, emits, and anisotropically scatters thermal radiation. At $x<0$, the walls are also at T_0 (also set equal to zero), and the wall temperature is suddenly increased to T_w at $x \geq 0$. When pure forced convection with large Peclet number is considered, only the y-direction conduction is included in the analysis, and the fluid thermal development can be followed downstream until it becomes fully developed.[3]

The effect of adding a one-dimensional radiation contribution in the y direction has been extensively studied for this geometry. Chawla and Chan[4] report on thermally developing Poiseuille flow results for isotropically scattering gray medium, using a numerically exact one-dimensional radiation analysis. Mengüc et al.[5] also report solutions including the effect of diffuse and specular reflecting walls. Lee and Buckius[6] report results using a scaled one-dimensional radiation solution and consider full thermal development of such flows with radiation.[7]

Including only the one-dimensional radiation is very questionable at the channel entrance. Here, the fluid exchanges energy by radiation with the walls at T_0 and T_w simultaneously.

This entrance two-dimensional effect is characteristic of radiative transfer in this flow configuration and must be included. Kobiyama et al.[8] report on the two-dimensional radiative effects when laminar and turbulent flows of purely absorbing gray fluids pass through a finite heating section with a constant wall temperature. A two-dimensional radiation effect can also be important when an applied wall heat flux and conduction along the walls results in a variable wall temperature distribution.[9]

Two-dimensional radiation effects on laminar or turbulent flows in circular pipes have been considered by many investigators.[10-13] Einstein[10] considered the two-dimensional radiation effect on a pure absorbing fluid with heat generation. Pearce and Emery[11] solve the thermal entry problem of gray and approximately nongray absorbing fluid. Echigo et al.[12] report on the two-dimensional preheating effect of a gray absorbing fluid in a thermally developing pipe. Smith et al.[13] solve the combined heat transfer for a tube flow (laminar or turbulent) with a finite length, where the medium is assumed to be nongray absorbing and isotropically scattering.

The effect of two-dimensional radiation on anisotropic scattering media has not been previously considered in either the circular pipe or the plane parallel channel geometry. In this study, the two-dimensional entrance effect for anisotropically scattering fluids is considered for a plane channel flow. The effects of the phase function, scattering albedo, channel optical height, diffuse wall reflectivity, and conduction-radiation parameter on the heat transfer and temperature development in the channel are investigated.

The importance of radiative preheating of the absorbing-scattering fluid is examined by comparing the results from two different computation domains. The domain (a) in Figs. 1b and 1c is the same computation domain considered for one-dimensional radiation studies[4-7] and for some two-dimensional radiation studies.[8,10-13] The domain (b) in Fig. 1c is similar to the domain considered in Ref. 8 for a channel flow and in Ref. 12 for a circular pipe flow. This domain extends a length L_e before the domain (a), where the fluid preheating takes place.

Governing Equations

The appropriate nondimensional energy equation is written in the transformed optical coordinates of τ_x and τ_y.

$$u^*(\tau_y)\frac{\partial T^*(\tau_x,\tau_y)}{\partial \tau_x} = \frac{2\tau_{yH}}{Pe}\left[\frac{\partial^2}{\partial \tau_x^2}+\frac{\partial^2}{\partial \tau_y^2}\right]T^*(\tau_x,\tau_y) - \frac{2\tau_{yH}}{Pe}\frac{(1-\omega)}{N_{cr}}\left[T^{*4}(\tau_x,\tau_y)-G^*(\tau_x,\tau_y)\right] \quad (1)$$

The streamwise convection term is balanced by the streamwise and cross-stream conduction terms and the two-dimensional radiation contribution. A fully developed velocity profile for the Poiseuille flow is given by

$$u^*(\tau_y) = 6[\tau_y/\tau_{yH} - (\tau_y/\tau_{yH})^2] \quad (2)$$

The properties of the medium are assumed to be constant, and viscous dissipation is not included.

The boundary conditions for the energy equation are:

For domain (a) with no preheating (Fig. 1c)

$$T^* = 1, \qquad \text{at } \tau_y = 0 \text{ and } \tau_{yH}, \text{ for } \tau_x \geq 0 \quad (3a)$$

$$T^* = 0, \qquad \text{at } \tau_x = 0, \text{ for } 0 \leq \tau_y \leq \tau_{yH} \quad (3b)$$

For domain (b) with preheating (Fig. 1c)

$$T^* = 1, \qquad \text{at } \tau_y = 0 \text{ and } \tau_{yH}, \text{ for } \tau_x \geq 0 \quad (3a)$$

$$T^* = 0, \qquad \text{at } \tau_y = 0 \text{ and } \tau_{yH}, \text{ for } \tau_x < 0 \quad (3c)$$

$$T^* = 0, \qquad \text{at } \tau_x = -\tau_e, \text{ for } 0 \leq \tau_y \leq \tau_{yH} \quad (3d)$$

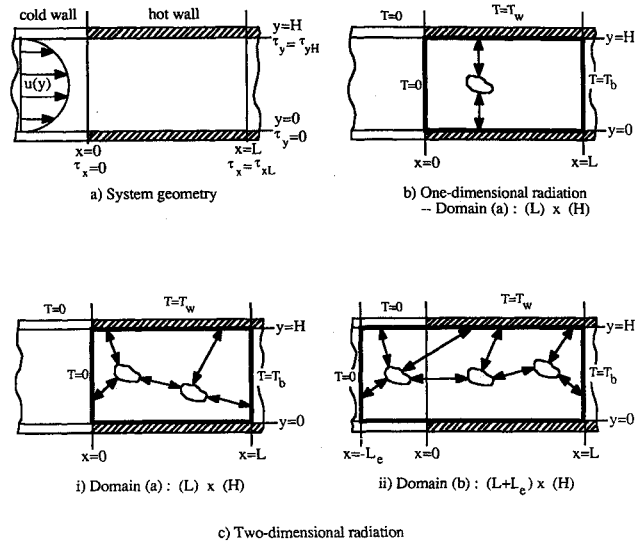

Fig. 1 System geometry and boundary conditions.

The extended x dimension of the calculation domain τ_e is taken to be the length at which the intensity originating from $x = 0$ would be reduced to at least 1% of the original value when Beer's law is applied in the x direction. The τ_e thus chosen should be sufficient for studying any radiative interaction upstream of $x = 0$, and the boundary condition in Eq. (3d) can also be justified. For the results presented in this work, τ_e is taken to be 5 for $\tau_{yH} \leq 2$ and 10 for $2 < \tau_{yH} \leq 5$.

At the exit of an infinite plane parallel channel ($x = \infty$), the fluid temperature should be equal to the wall temperature, and $\partial T/\partial x$ is zero. Incorrectly specifying the zero derivative condition at the exit of a finite x computation domain can cause some unrealistic numerical results near the exit region. The exit boundary condition can be more accurately specified by allowing for slight changes in the fluid temperature near the exit. Since small changes in temperature can be accurately approximated by a linear profile, the exit boundary condition is expressed as

$$\frac{\partial^2 T^*}{\partial \tau_x^2} = 0, \qquad \text{at } \tau_x = \tau_{xL}, \text{ for } 0 \leq \tau_y \leq \tau_{yH} \quad (3e)$$

The length of the computation domain (τ_{xL}) needs to be sufficiently long to allow for a nearly complete heating of the fluid to meet the boundary condition specified in Eq. (3e). The channel length required for sufficient heating is dependent on both τ_{yH} and Pe. It was found that when the similarity parameter $\zeta (= 2\tau_x\tau_{yH}/Pe)$ is larger than 1, the fluid temperatures are usually very close to the wall temperature near the exit boundary. For all cases considered, $\tau_{xL} = 15$ is sufficient to ensure adequate heating that results in smoothly developing temperature profiles. Increasing the τ_{xL} beyond this length did not influence the solution.

The radiative contribution to the energy equation is evaluated by solving the radiative transfer equation for an absorbing, emitting, and anisotropically scattering medium given by

$$\left[\mu\frac{\partial}{\partial \tau_x}+\xi\frac{\partial}{\partial \tau_y}+1\right]I^*(\tau_x,\tau_y,\Omega) = S^*(\tau_x,\tau_y,\Omega) \quad (4)$$

where

$$S^*(\tau_x,\tau_y,\Omega) = (1-\omega)T^{*4}(\tau_x,\tau_y) + \frac{\omega}{4\pi}\int_{\Omega'} I^*(\tau_x,\tau_y,\Omega')\Phi(\Omega';\Omega)d\Omega' \quad (5)$$

The "′" indicates incident direction, and (μ,ξ) are the direction cosines in x and y directions that describe the direction Ω. The scattering phase function is approximated by a finite series of Legendre polynomials as

$$\Phi(\Omega';\Omega) = \Phi(\cos\psi) \simeq \sum_{\ell=0}^{K} C_\ell P_\ell(\cos\psi) \tag{6}$$

where $(K+1)$ is the number of terms used to approximate the phase function.

The two channel walls emit at the specified wall temperature and diffusely reflect incoming radiation ($\rho = 1 - \epsilon_w$). The inlet and outlet of the computation domain are treated as pseudoblack walls ($\rho = 0$, $\epsilon_w = 1$) with prescribed temperatures. At the inlet, the fluid temperature is considered to zero. The temperature at the exit pseudoblack wall is assumed to be

$$T^* = T_b^*, \qquad \text{at } \tau_x = \tau_{xL}, \text{ for } 0 \le \tau_y \le \tau_{yH} \tag{7}$$

where the fluid bulk temperature is determined by

$$T_b^*(\tau_x) = \frac{\int_0^{\tau_{yH}} u^*(\tau_y) T^*(\tau_x,\tau_y)\mathrm{d}\tau_y}{\int_0^{\tau_{yH}} u^*(\tau_y)\mathrm{d}\tau_y} \tag{8}$$

The pseudoblack inlet and exit assumptions are easily justified for this infinite channel problem, since a uniform temperature, optically thick fluid radiates like a black wall. The fluid before the inlet is isothermal, and the fluid beyond the exit is also nearly isothermal, since τ_{xL} must be long to meet the boundary condition of Eq. (3e). The intensities from any of the four boundaries can be written as

$$I_w^*(\tau_x,\tau_y,\Omega) = \epsilon_w T^{*4}(\tau_x,\tau_y)|_{\text{wall}} + \frac{\rho}{\pi}\int_{n\cdot\Omega'<0} |n\cdot\Omega'| I_w^*(\tau_x,\tau_y,\Omega')\mathrm{d}\Omega', \qquad \text{for } n\cdot\Omega>0 \tag{9}$$

Once the dimensionless intensity field is obtained, the dimensionless average incident radiation, needed as a source term in the energy equation, is obtained as

$$G^*(\tau_x,\tau_y) = \frac{1}{4\pi}\int_{4\pi} I^*(\tau_x,\tau_y,\Omega)\mathrm{d}\Omega \tag{10}$$

The net radiative heat flux at a wall can also be obtained by using the intensity solution as

$$Q_{rw}^*(\tau_x) = \frac{1}{\pi}\int_{4\pi} \xi I^*(\tau_x,\tau_y=0,\Omega)\mathrm{d}\Omega \tag{11}$$

The energy and the radiative transfer equations, together with the boundary conditions, give a complete description of the heat transfer. The energy equation is solved by using the SIMPLE code developed by Patankar.[14] The radiation term in the energy equation is treated as a temperature-dependent source term, and it is linearized as recommended in Ref. 14. The two-dimensional radiative transfer is solved by using the S-8 discrete ordinates method,[1] which computes 40 fluxes over a unit hemisphere. Accuracy of high-order S-N discrete ordinates method has been demonstrated in our previous study,[1] where the solutions for isotropic scattering media have been compared against previously published results. The accuracy of the anisotropic scattering results is assured by accurate phase function normalization and energy balance. Although S-14 results were presented as benchmark solutions in Ref. 1, S-8 solutions were also shown to be very accurate with negligibly small ray effect even for pure absorbing medium.

The calculation domain is subdivided into small control volumes. The grid points are placed on the Lobatto quadrature points in the y direction. Exponentially varying grid locations are used for the x direction, where a finer grid is placed near $x = 0$. Number of grid points used are

1) For $\tau_{yH} = 2$:

$$(\tau_{xL})_{\text{Total}} = \tau_e + \tau_{xL} = 5 + 15$$

$$MY = 27, \qquad MX_{\text{Total}} = MX_e + MX = 10 + 41$$

2) For $\tau_{yH} = 5$:

$$(\tau_{xL})_{\text{Total}} = \tau_e + \tau_{xL} = 10 + 15$$

$$MY = 35, \qquad MX_{\text{Total}} = MX_e + MX = 20 + 41$$

Using a larger number of grid points in the x direction did not result in any improvements, and the y direction grids have also been shown to be fine enough for accuracy in predicting the radiative transfer.

Since the energy and radiative transfer equations are coupled in a nonlinear fashion, iterations between the two codes are necessary. Two convergence tests are separately applied to the solutions of energy and radiative transfer equations. A third convergence test checks the combined final temperature results. The three convergence tests are the following:

1) SIMPLE code: Solves the finite-differenced energy equation by using the iterative Gauss-Seidel method for a given radiation source input. The initial temperature field in the channel is supplied as a linear profile along x, which gives $T^* = 0$ at $\tau_x = -\tau_e$ and $T^* = 1$ at $\tau_x = -\tau_{xL}$. In this study, 40 iterations were used, which resulted in energy balance errors less than 10^{-5}.

2) S-N discrete ordinates code: Given a temperature profile, the S-N method solves the equation of transfer iteratively for the intensity field. The initial intensity field is supplied as zero, and the convergence criterion is applied as

$$\text{Maximum } (I_{\text{old}} - I_{\text{new}})/I_{\text{old}} \le 10^{-7} \tag{12a}$$

With this criterion, the radiative energy-balance error in the control volumes becomes less than 10^{-7}.

3) A new temperature solution is obtained by the SIMPLE code with the radiation-source-term result from test 2. The convergence criterion used for stopping the iteration between the SIMPLE and S-N codes is

$$\text{Maximum } (T_{\text{old}} - T_{\text{new}})/T_{\text{old}} \le 10^{-7} \tag{12b}$$

Typical computer times required for the solutions are about 250 s for $\tau_{yH} = 2$ and 400 s for $\tau_{yH} = 5$ on Cray 2 with isotropic scattering media. For anisotropic scattering media, the required computer times are 250–500 s for $\tau_{yH} = 2$ and 700–1200 s for $\tau_{yH} = 5$, respectively.

Results and Discussions

From the solutions of the intensity and temperature fields, bulk temperature, normalized temperature profile, and net radiative wall heat flux are presented to illustrate the heat transfer in the channel. The effects of Pe, N_{cr}, ρ, and the phase function anisotropy on the heat transfer are studied. The Legendre polynomial series-expansion coefficients of the scattering phase functions used for this study are given in Table 1. F indicates forward scattering phase functions, and B indicates backward scattering phase functions. The isotropic scattering phase function has only $C_0 = 1$, and its asymmetry factor is zero. Detailed information about these phase functions can also be found in Kim and Lee.[1,2]

Figure 2 shows a comparison between a normalized temperature field that results from a pure convection situation (Fig. 2a) and that which results from a combined strong radiation-convection situation (Fig. 2b). The fluid temperatures across

Table 1 The phase function expansion coefficients C_ℓ

ℓ	$F1$	$F2$	$B2$
0	1.00000	1.00000	1.00000
1	2.53602	2.00917	−1.20000
2	3.56549	1.56339	0.50000
3	3.97976	0.67407	
4	4.00292	0.22215	
5	3.66401	0.04725	
6	3.01601	0.00671	
7	2.23304	0.00068	
8	1.30251	0.00005	
9	0.53463		
10	0.20136		
11	0.05480		
12	0.01099		
Number of terms	13	9	3
f	0.84534	0.66972	−0.40000

the channel width of $\tau_y = 2$ are shown developing in the τ_x direction, where the sudden wall temperature change from zero to one occurs at $\tau_x = 0$. The $\omega = 1$ solution in Fig. 2a is equivalent to a pure convection solution, since such a medium is unable to absorb any thermal radiation. The pure convection temperature field shows nearly no preheating since for $Pe = 50$ the streamwise conduction is very small. The thermal development in the heated section of the channel is also slow without radiation. For a strong radiation problem of $N_{cr} = 0.01$ and $\omega = 0.5$ with anisotropic scattering phase function $F1$ (Fig. 2b), there is significant preheating in the extended region which is mainly due to the two-dimensional radiation effect. The thermal development of the fluid is noticeably rapid with strong radiation.

Figure 3 shows how strong radiation effects change the dimensionless similarity temperature profiles for the same cases considered in Fig. 2. The dimensionless temperature profiles $[\theta = (T_w - T)/(T_w - T_b)]$ for $\omega = 1$ (no radiation case) on the left-hand side of the figure show that the dimensionless temperature profiles are becoming self-similar as $\zeta > 0.2$. On the right-hand side of the figure, the dimensionless temperature profiles for $\omega = 0.5$ with $F1$ phase function are shown. The fluid thermal development in the extended entrance region ($\tau_x < 0$, $\zeta < 0$) is also examined, where the dimensionless temperature is simply $\theta = T^*/T_b^*$ because $T_w^* = 0$ in this region. Notice the very different temperature profiles for ζ near 0 ($\zeta = -0.079$ and $\zeta = 0.0013$). The dimensionless temperature profiles become smoother and appear nearly self-similar as ζ is further increased.

Figure 4 show comparisons of the bulk temperature results obtained from a one-dimensional radiation analysis, a two-dimensional radiation analyses without preheating domain [2-D(a)] and a two-dimensional radiation analysis with preheating domain [2-D(b)]. The one-dimensional radiation solution is only dependent on the temperature distribution at one x location (see Fig. 1b), and the net x direction radiative flux at that location is always zero. The two-dimensional radiation solutions are dependent on the temperature distribution over the entire computation domain (see Fig. 1c). The normalized temperature field for the two-dimensional solution with the preheating region (calculation domain b) was shown in Fig. 2b. The corresponding bulk temperature development shown in Fig. 4 clearly shows that the cold fluid undergoes about 50% of the heating before x = 0 where the walls actually become hot.

There is relatively little difference in the T_b^* between the one-dimensional result and the two-dimensional result without preheating domain (calculation domain a). This is because neither analysis allows for radiative interactions between the hot-walled region at $x \geq 0$ and the cold-walled region at $x < 0$. Both the two-dimensional analyses do allow for radiative exchange between the cold incoming fluid and the hot fluids downstream. This exchange causes the less rapid bulk temperature developments shown for the two-dimensional results in Fig. 4. Far downstream, the effect of the cold-walled section becomes weak, and the two-dimensional solutions 2-D(a) (without preheating domain) and 2-D(b) (with preheating domain) show nearly the same T_b^*. Since the two-dimensional treatment of radiation including the upstream preheating results in the most realistic solutions, only such solutions are considered in this study.

The strong radiation effects shown in Figs. 2–4 are characterized by a small value of the conduction-radiation parameter

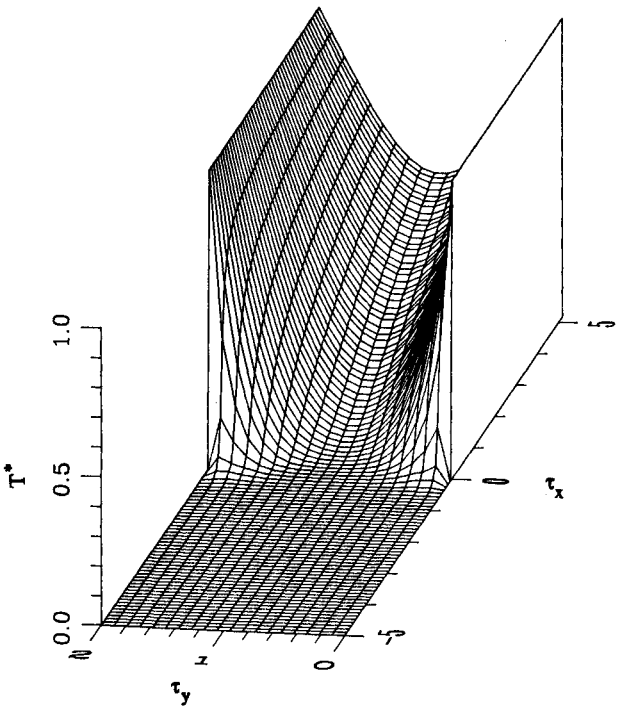

a) ω = 1.0 (No radiation effect)

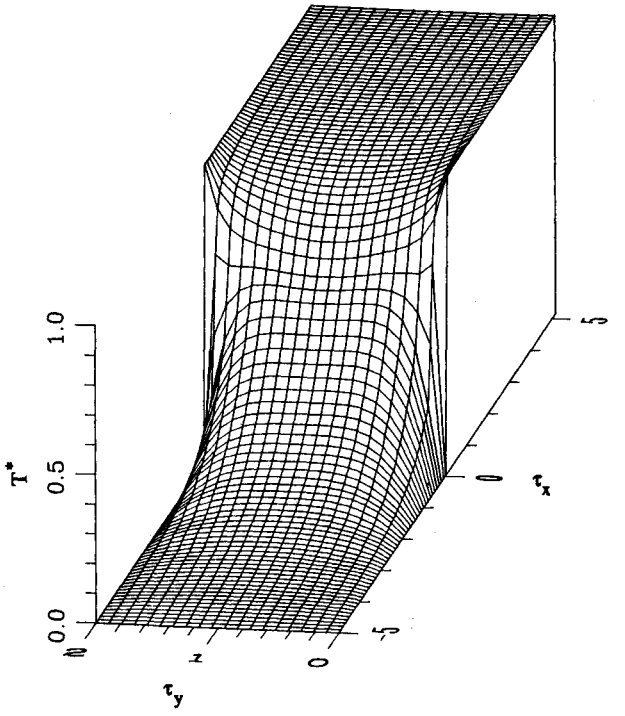

b) ω = 0.5 and phase function F1

Fig. 2 Dimensionless temperature profiles: a) $\omega = 1$ and b) $\omega = 0.5$ with $F1$ ($N_{cr} = 0.01$, $\rho = 0$, $\tau_{yH} = 2$, and $Pe = 50$).

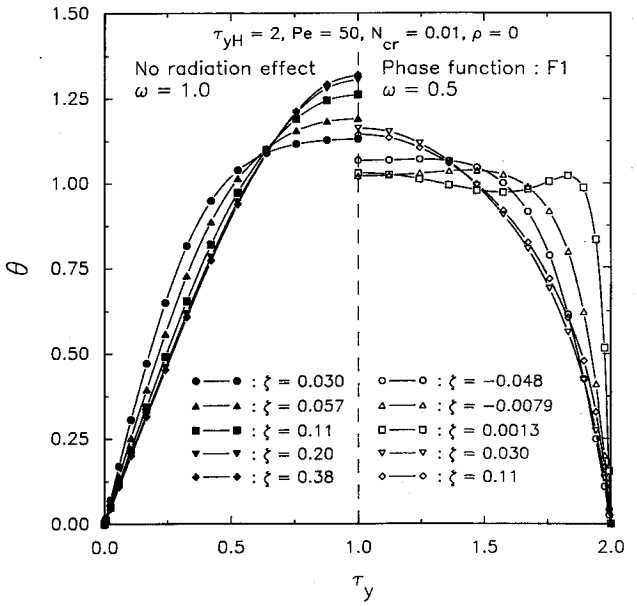

Fig. 3 Similarity temperature profiles.

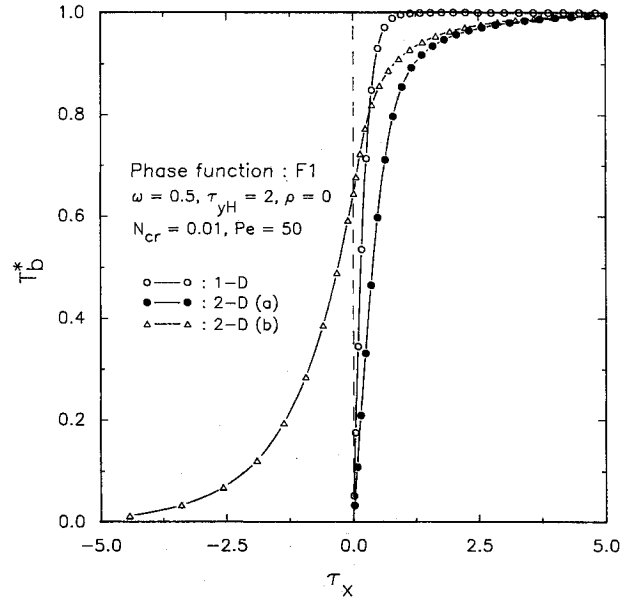

Fig. 4 Bulk temperature comparison between one- and two-dimensional radiation solutions.

N_{cr}. The effect of N_{cr} on the fluid bulk temperature is shown in Fig. 5 for a different phase function $F2$ with $\omega = 0.5$. For a relatively large N_{cr} of 0.5, the radiation contribution term in Eq. (1) is small as compared to the convection and cross-stream conduction terms, and the resulting upstream preheating is very small. In this case, the total Nusselt number, which includes the effects of the convection and radiation, reaches an asymptotic value that is nearly the pure convection heat-transfer result of 7.541. Then, the streamwise bulk temperature distribution shown in Fig. 5 also resembles the pure convection result. For N_{cr} of 0.1, the radiation contribution is still small, but the preheating and thermal development are slightly increased as compared to the $N_{cr} = 0.5$ results. When N_{cr} is further decreased to 0.01, the radiative contribution to the heat transfer is quite strong, and Fig. 5 shows a significant preheating of the fluid, which is due to the two-dimensional radiation effect. The small amounts of preheating for the larger N_{cr} cases is due primarily to upstream conduction and not to two-dimensional radiation. Since the current study seeks to examine the effect of two-dimensional radiation preheating in a combined mode heat-transfer problem, only N_{cr} of 0.01 is considered for the rest of the results presented.

All of the results discussed thus far have been for the case of $Pe = 50$. The effect of the Peclet number on the developing bulk temperatures is shown in Fig. 6 for the $F2$ phase function with $\omega = 0.5$. For small Peclet numbers, the heat transfer in the channel is dominated by conduction and radiation, and the convection term becomes relatively unimportant in Eq. (1). Because of this large conduction and radiation effect, the fluid in the extended entrance region is significantly heated before flowing into the heated section. For $Pe = 1$ or 10, the preheated bulk fluid temperature reaches up to 85% of the hot wall temperature before entering the heated section. As the Peclet number increases, the preheating effect becomes less important since the conduction and the radiation terms in Eq. (1) become relatively less important. For $Pe = 500$, the preheating of the fluid in the entrance extended region is very small (5%), and convection is dominant as compared to the other two heat-transfer modes. Radiation, convection, and

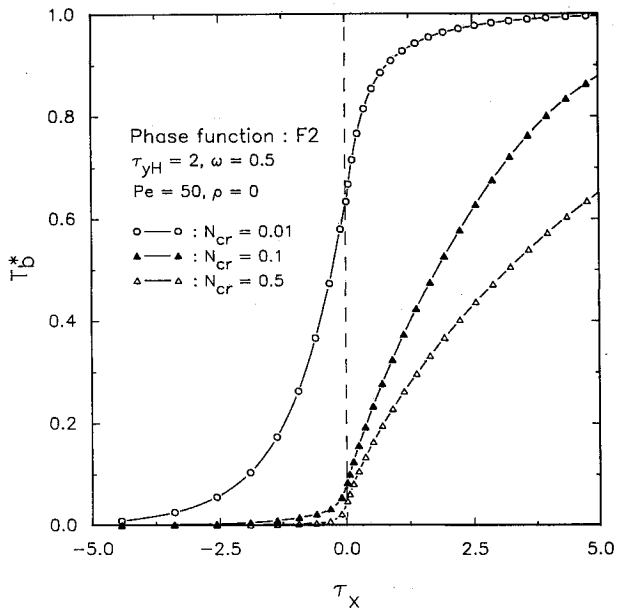

Fig. 5 Effect of the conduction-radiation parameter on the bulk temperature.

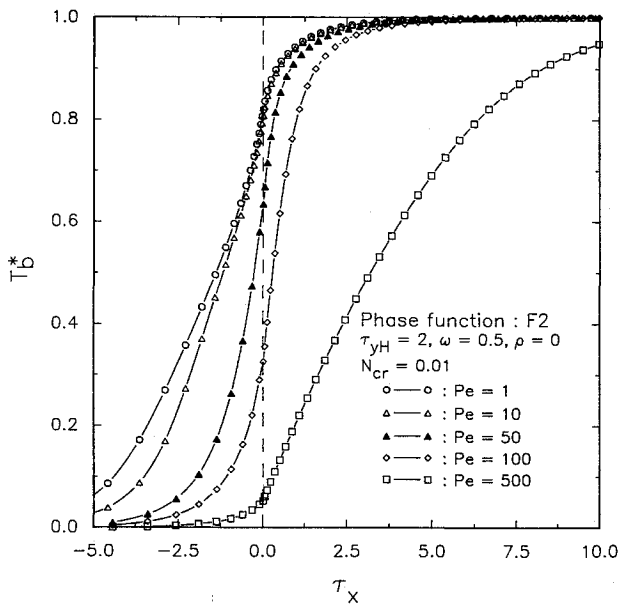

Fig. 6 Effect of the Peclet number on the bulk temperature.

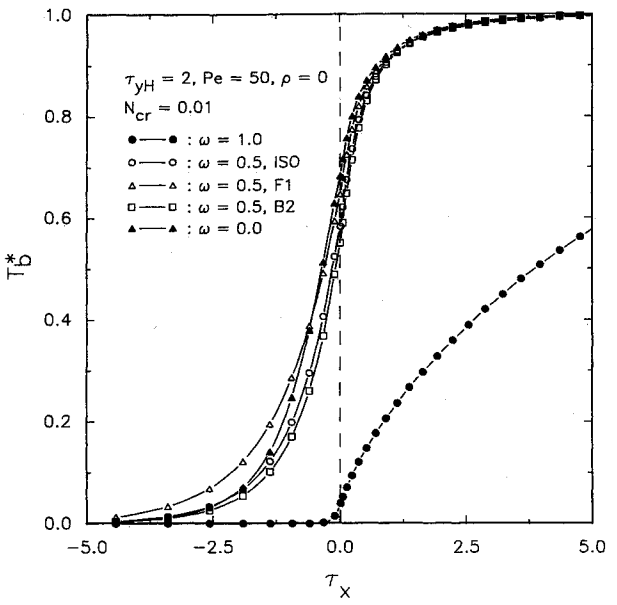

Fig. 7 Effect of scattering albedo on the bulk temperature.

conduction terms are all important for the $Pe = 50$ case that is considered in all other figures in this section, although most of the preheating is still due to the two-dimensional radiation rather than upstream conduction.

Figure 7 shows the importance of the scattering albedo and the phase functions on the bulk temperature development. When $\omega = 1.0$, the medium scatters but does not absorb any radiation. The slow thermal development of the purely scattering fluid is equivalent to that of the pure convection situation, and the preheating of about 3% before $x = 0$ is due to the upstream conduction. As absorption becomes more important compared to scattering (decreasing ω), the characteristic upstream preheating becomes apparent. The thermal development is also more rapid for an absorbing medium in the preheating section. For the pure absorbing medium with $\omega = 0$, the preheating of the extended entrance region is very significant, and the entering fluid into the heated section experiences 70% preheating before $x = 0$. For the intermediate albedo of 0.5, three different phase functions are considered. For the isotropic scattering or the backward scattering ($B2$ phase function) medium, the amount of preheating at $x = 0$ and thermal penetration upstream are both less than those for the $\omega = 0$ case. For the forward scattering $F1$ phase function with $\omega = 0.5$, the thermal penetration is more significant than that for $\omega = 0$. The medium with the forward scattering $F1$ phase function scatters more of the emitted energy from the hot walls and hot fluid downstream to the upstream cold fluid.

The effect of the scattering phase functions and the channel optical height on the T_b^* and the Q_{rw}^* distributions is shown in Figs. 8 and 9 for $\omega = 0.5$. Figure 8 shows that the forward scattering phase functions $F1$ and $F2$ result in more upstream preheating and deeper thermal penetration into the upstream, while the backward scattering phase function $B2$ with the smaller asymmetry factor results in less preheating, as compared to the isotropic scattering. The preheating and thermal penetration are also a strong function of the phase function anisotropy as we see from the results of the $F1$ and $F2$. The phase function $F1$ with the larger asymmetry factor results in more upstream preheating and thermal penetration as compared to the phase function $F2$ with the smaller asymmetry factor.

The effect of the scattering phase functions on the thermal development is more pronounced for large $\tau_{yH} = 5$ than for $\tau_{yH} = 2$. The larger optical thickness layer at the extended entrance region absorbs more of the thermal energy from the hot walls and fluids downstream rather than letting it pass out to the cold walls. This causes a significant increase of the medium temperature in the preheating section for $\tau_{yH} = 5$.

In the far downstream hot wall section at large x, the boundary conditions become increasingly symmetric, and the effect of the different scattering phase functions on the bulk temperature is canceled out. The resulting solutions all resemble the isotropic scattering solution. This insensitivity to the shape of the phase functions is more pronounced for the smaller τ_{yH} channel, since the cold inlet region is only a small portion of the whole boundary.

The cold wall net radiative heat flux in Fig. 9 ($\tau_x < 0$) shows that the forward scattering media are able to transmit more of the radiation from the hot walls to the cold fluids, and the resulting higher T_b^* gives the most negative Q_{rw}^* for the $F1$ media. In the hot wall section ($\tau_x > 0$), the net wall flux is larger for the larger τ_{yH} media, partly because the bulk temperatures are lower. Another effect is that as the τ_{yH} increases, both the effect of the cold walls and the inlet boundary with the cold entering fluid affect the heat transfer from the hot region.

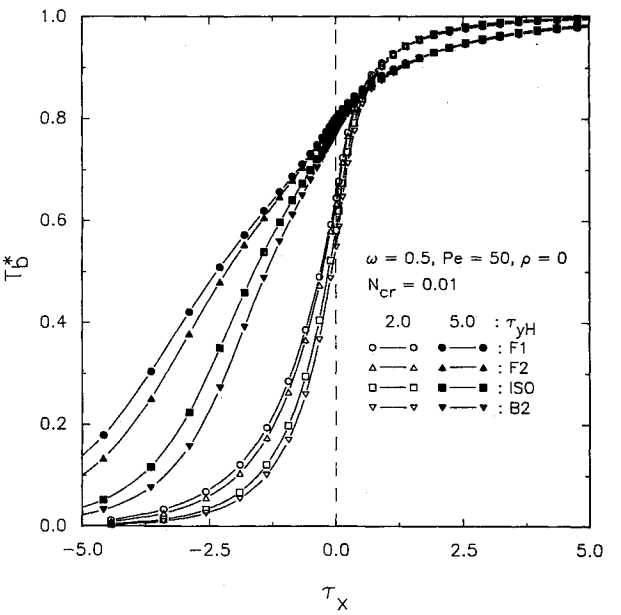

Fig. 8 Effects of scattering phase function and optical depth on the bulk temperature.

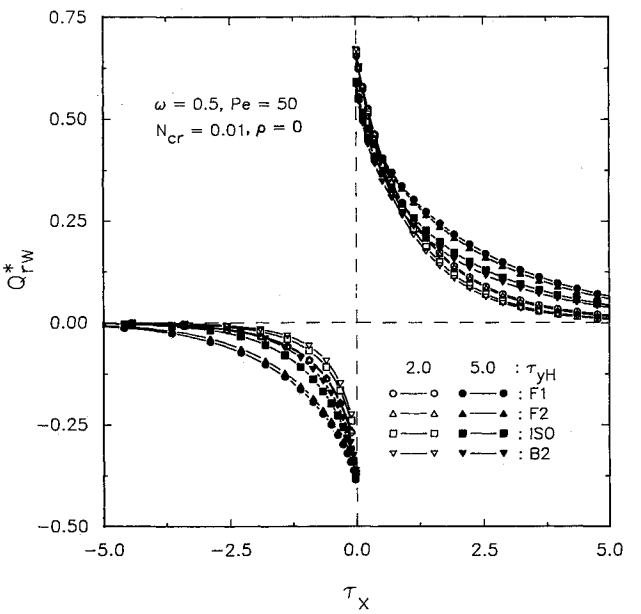

Fig. 9 Net wall radiative flux.

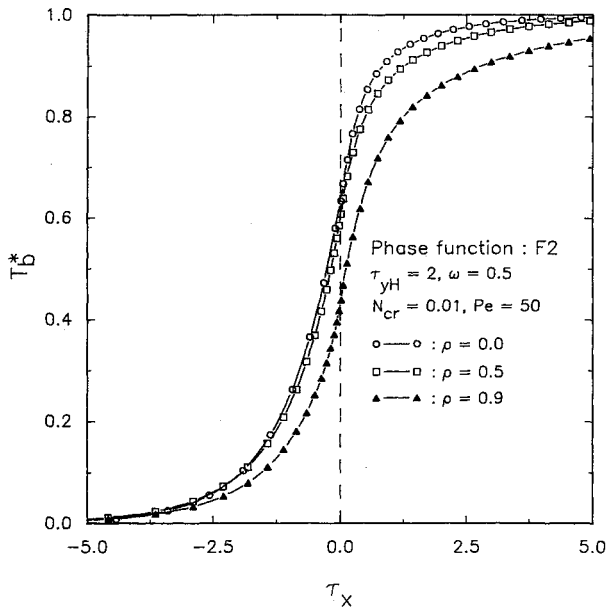

Fig. 10 Effect of the diffuse wall reflectivity on the bulk temperature.

Figure 10 shows the effect of the diffuse wall reflectivity on the fluid bulk temperature development. The $F2$ phase function is considered for $\omega = 0.5$. The three different diffuse wall reflectivities, $\rho = 0$, 0.5, and 0.9, represent large differences in the input radiative energies. Radiative heat flux σT_w^4 for $\rho = 0$ is reduced to 50% for $\rho = 0.5$ and 10% for $\rho = 0.9$. Even for the smallest radiation input, the bulk temperature development can be dramatically different from that for a no-radiation solution when the medium absorbs and scatters radiation ($\omega = 1$ curve of Fig. 7). For highly reflecting walls, the fluid can be heated up with less amount of radiative energy input as compared to the low-reflecting walls. The bulk temperature development for $\rho = 0.9$ shows 43% preheating at $\tau_x = 0$ compared to 70% for isotropic scattering medium shown in Fig. 7.

Summary and Conclusions

The combined mode heat transfer in thermal entry region of channel flow must be analyzed by including two-dimensional radiative transfer and by taking the upstream preheating and anisotropic scattering effects into account. Approximating the radiation as one-dimensional or treating a two-dimensional radiation without preheating gives unacceptable results, particularly for highly absorbing media and for large optical depths. For an anisotropic scattering medium with $F1$ phase function for $\tau_{yH} = 2$ and $\omega = 0.5$ ($N_{cr} = 0.01$, $Pe = 50$, $\rho = 0$), preheating of the entering fluid reaches up to 65% of the specified hot wall temperature before entering the heated section. For the same phase function with $\tau_{yH} = 5$ and $\omega = 0.5$, the preheating reaches up to 81%, and the thermal penetration upstream reaches up to an optical depth of 10 before $\tau_x = 0$. The reflecting walls enhance the fluid thermal development significantly even with small radiative energy input.

Acknowledgments

This work was supported, in part, by the National Science Foundation Grant NSF/CBT-8451076. A grant from the Minnesota Supercomputer Institute is also gratefully acknowledged.

References

[1]Kim, T.-K., and Lee, H., "Effect of Anisotropic Scattering on Radiative Heat Transfer in Two-Dimensional Rectangular Enclosures," *International Journal of Heat and Mass Transfer,* Vol. 31, No. 8, 1988, pp. 1711–1721.

[2]Kim, T.-K., and Lee, H., "Radiative Transfer in Two-Dimensional Anisotropic Scattering Media with Collimated Incidence," *Journal of Quantitative Spectroscopy and Radiative Transfer,* Vol. 42, No. 3, 1989, pp. 225–238.

[3]Kays, W. M., and Crawford, M. E., *Convective Heat and Mass Transfer,* 2nd ed., McGraw-Hill, New York, 1980, Chap. 8.

[4]Chawla, T. C., and Chan, S. H., "Combined Radiation Convection in Thermally Developing Poiseuille Flow with Scattering," *Journal of Heat Transfer,* Vol. 102, No. 2, 1980, pp. 297–302.

[5]Mengüc, M. P., Yener, Y., and Özisik, M. N., "Interaction of Radiation in Thermally Developing Laminar Flow in a Parallel-Plate Channel," American Society of Mechanical Engineers, New York, 83-HT-35, 1983.

[6]Lee, H., and Buckius, R. O., "Combined Mode Heat Transfer Analysis Utilizing Radiation Scaling," *Journal of Heat Transfer,* Vol. 108, No. 3, 1986, pp. 626–632.

[7]Lee, H., Chikh, S., and Ma, Y., "Full Thermal Development of Radiatively Participating Media in Poiseuille Flow," AIAA Paper 88-2724, 1988.

[8]Kobiyama, M., Taniguchi, H., and Saito, T., "The Numerical Analysis of Heat Transfer Combined with Radiation and Convection," *Bulletin JSME,* Vol. 22, No. 167, 1979, pp. 707–714.

[9]Kassemi, M., and Chung, B. T. F., "Conjugated Heat Transfer of a Radiatively Participating Gas in a Channel," *Proceedings of the Eighth International Heat Transfer Conference,* Vol. 2, 1986, pp. 797–802.

[10]Einstein, T. H., "Radiant Heat Transfer to Absorbing Gases Enclosed in a Circular Pipe with Conduction, Gas Flow, and Internal Heat Generation," NASA TR R-156, 1963.

[11]Pearce, B. E., and Emery, A. F., "Heat Transfer by Thermal Radiation and Laminar Forced Convection to an Absorbing Fluid in the Entry Region of a Pipe," *Journal of Heat Transfer,* Vol. 92, No. 2, 1970, pp. 221–230.

[12]Echigo, R., Hasegawa, S., and Kamiuto, K., "Composite Heat Transfer in a Pipe with Thermal Radiation of Two-Dimensional Propagation—in Connection with the Temperature Rise in Flowing Medium Upstream from Heating Section," *International Journal of Heat and Mass Transfer,* Vol. 18, No. 10, 1975, pp. 1149–1159.

[13]Smith, T. F., Byun, K.-H., and Ford, M. J., "Heat Transfer for Flow of an Absorbing, Emitting, and Isotropically Scattering Medium Through a Tube with Reflecting Walls," *Proceedings of the Eighth International Heat-Transfer Conference,* Vol. 2, 1986, pp. 803–808.

[14]Patankar, S. V., *Numerical Heat Transfer and Fluid Flow,* McGraw-Hill, New York, 1980, Chaps. 4 and 6.